Journal of Molecular Structure 1248 (2022) 131468

Contents lists available at ScienceDirect

Journal of Molecular Structure

journal homepage: www.elsevier.com/locate/molstr

Photoluminescence of pefloxacindi-ium manganese(II) and zinc(II) tetrahalides

Nicolay N. Golovnev[a], Marina A. Gerasimova[a], Maxim S. Molokeev[a,b,c,d,*], Mikhail E. Plyaskin[a], Mikhail E. Baronin[a]

[a] Siberian Federal University, 79 Svobodny Prospect, Krasnoyarsk 660041, Russia
[b] Laboratory of Crystal Physics, Kirensky Institute of Physics, Federal Research Center KSC SB RAS, bld. 38 Akademgorodok 50, Krasnoyarsk 660036, Russia
[c] Department of Physics, Far Eastern State Transport University, 47 Seryshev Str., Khabarovsk 680021, Russia
[d] Research and Development Department, Kemerovo State University, 6 Krasnaya Str., Kemerovo 650000, Russia

ARTICLE INFO

Article history:
Received 12 May 2021
Revised 1 September 2021
Accepted 7 September 2021
Available online 17 September 2021

Keywords:
Manganese and zinc halides
Pefloxacin
Ionic compounds
Photoluminescence
X-ray diffraction
Thermal decomposition

ABSTRACT

Mn^{2+}-based hybrid materials have become the hotspot of current research studies owing to their high photoluminescence quantum yield (PLQY), low-cost, environmental friendliness and stability. For the first time, we report the hydrothermal synthesis of two lead-free zero-dimensional luminescent organic-inorganic hybrid compounds, $PefH_2[MnBr_4]$ (**1**) and $PefH_2[MnCl_4]$ (**2**) (Pef = pefloxacin). They were characterized by elemental analysis, TG-DSC, single-crystal and powder XRD. Compounds **1**–**2** exhibit a distorted tetrahedral geometry around the manganese(II) metal center, which is isolated from the same centers by bulky pefloxacindi-ium ($PefH_2^{2+}$) ions with a Mn···Mn distance of 7.3 Å. Their structures are stabilized by N—H···O, O—H···X (X = Br, Cl), C—H···O and C—H···X hydrogen bands and $\pi-\pi$ stacking interaction. Thermal decomposition starts at $T > 230$°C for **1** and $T > 210$°C for **2** and proceeds for several stages. Upon UV excitation compounds exhibit a bright green emission with a moderate PLQY of 45% for **1** and 30% for **2**. The influence of the halide ion and metal ion on the photoluminescence properties of isostructural compounds $PefH_2[MX_4]$ (M = Mn, Zn and X = Br, Cl) is discussed.

1. Introduction

Organic-inorganic hybrid metal halides (HMHs), as a new class of functional materials, have been widely expanded due to their unique advantages, such as solution-process, low cost, large-scale production. Among them, lead(II) based HMHs have made great progress in solar energy conversion [1] and show superior bright and size-tunable photoluminescence [2–4]. Lead compounds are toxic, however, the use of lead should not preclude commercialization of hybrid lead halide compounds [5–7]. The development of lead-free HMHs is also highly desired. Mn-based HMHs can be considered as a very good alternative of lead compounds [8,9]. Although such compounds are well-known [10], they again attracted the attention of the researchers due to the high quantum yield, low cost, environmental friendliness, stability [11–21] and interesting ferroelectric/magnetic properties [22,23]. For the 0D organic-inorganic hybrid manganese(II) halides comprise isolated MnX_4^{2-} (X = Br, Cl) anions surrounded by the bulky organic cations, the photoluminescence quantum yield (PLQY) reaches up to 100% [16]. In comparison with the synthesis of Mn-based HMHs with a high quantum yield, great difficulties arise from the regulation of their optical properties. Various organic components and metal halide ions were used to achieve this goal, but the regulation is still a challenge. Weak absorption in the blue region due to the forbidden nature of d-d transitions requires new strategies of the material design based on the sensitization or enhancement of the spin-orbit coupling (SOC) effect [17]. To show trends in the change of photoluminescent properties, we chose four isostructural HMHs containing pefloxacin (Pef) in the form of a double charged $PefH_2^{2+}$ cation and Mn(II) or Zn(II) in the form of tetrachloride and tetrabromide anions. The bulkiness of this organic ion (Fig. 1) favors the crystallization of ionic compounds with isolated tetrahedral MX_4^{2-} (M = Mn, Zn; X = Br, Cl) units. Besides the ability to influence on photoluminescence (PL) of hybrid metal halides, $PefH_2^{2+}$ ion itself can also exhibit promising photoluminescent properties in solution [24] with potential application [25]. Unlike Mn(II), Zn(II) complexes show no emission originating from MLCT/LMCT excited states, since the Zn(II) ion is difficult to oxidize or reduce. The photoluminescence arises from

* Corresponding author at: Laboratory of Crystal Physics, Kirensky Institute of Physics, Federal Research Center KSC SB RAS, bld. 38 Akademgorodok 50, Krasnoyarsk 660036, Russia.
E-mail address: msmolokeev@gmail.com (M.S. Molokeev).

https://doi.org/10.1016/j.molstruc.2021.131468
0022-2860/

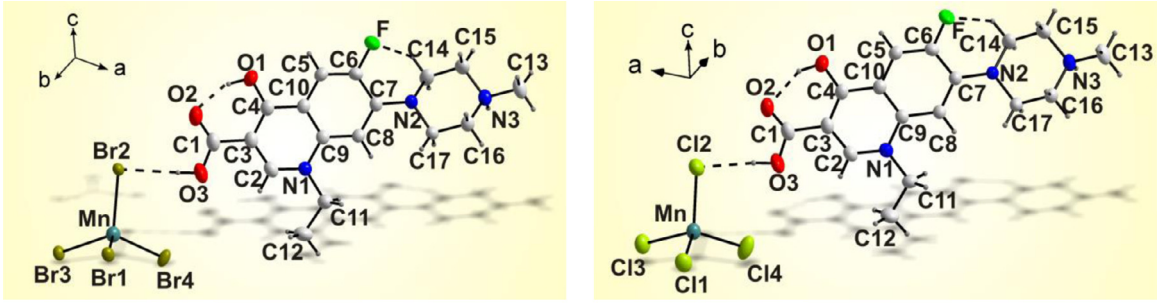

Fig. 1. Crystal structure of $PefH_2[MnBr_4]$ (a) and $PefH_2[MnCl_4]$ (b) in the asymmetric part of the unit cell, the hydrogen bonds are presented as dashed lines. The thermal ellipsoids are drawn at the 50% probability level.

intraligand electronic transitions, therefore the electronic properties (and thus luminescence) of Zn(II) complexes can be easily tuned by modification of the ligands [6,7]. Here, we propose the modification of photoluminescent properties of organic ions by assembly of organic $PefH_2^{2+}$ (pefloxacindi-ium) cations with manganese(II) and zinc(II) tetrahalides in HMHs. Two new hybrid manganese(II) halides, $PefH_2[MnBr_4]$ (**1**) and $PefH_2[MnCl_4]$ (**2**) are synthesized and their photoluminescent (PL) properties are investigated and compared to isostructural hybrid zinc(II) compounds, $PefH_2[ZnBr_4]$ (**3**) and $PefH_2[ZnCl_4]$ (**4**).

2. Experimental section

2.1. Reagents

Pefloxacin (CAS 70458-92-3, 3-carboxy-1-ethyl-6-fluoro-4-hydroxy-7-(4-methylpiperazin-4-ium-1-yl)quinolone) was obtained from Sigma-Aldrich. The reagents $MnBr_2{\cdot}4H_2O$, $MnCl_2{\cdot}4H_2O$, $ZnCl_2$, ZnO, HBr, HCl were of analytical grade. All chemicals were used without further purification.

2.2. Synthesis of crystals *1*-*4*

$PefH_2[MnBr_4]$ (**1**) and $PefH_2[MnCl_4]$ **(2)** were prepared by the crystallization from the aqueous solution of concentrated HCl and HBr at a molar ratio of MnX_2: Pef = 5:1. 0.30 g of pefloxacin was added to 3.0 ml of 8 M HBr (10 M HCl), then stoichiometric amount of solid $MnBr_2{\cdot}4H_2O$ ($MnCl_2{\cdot}4H_2O$) was added. The resulting solutions were evaporated to a volume of 1.5 ml and slowly cooled. The pale yellow and pale green crystals of **1** and **2** were filtered off and dried between sheets of filter paper in air at room temperature. The synthesized compounds are stable in air. The single crystals of compounds for the X-ray diffraction analysis were directly selected from the total mass of the corresponding precipitates. Yield of compounds **1**-**2** is 40-50%. The elemental analysis for $C_{17}H_{22}Br_4FMnN_3O_3$ (**1**): Calc.: C, 28.8%; H, 3.12%; N, 5.92%. Found: C, 28.5%; H, 3.27%; N, 5.77%. The elemental analysis for $C_{17}H_{22}Cl_4FMnN_3O_3$ (**2**): Calc.: C, 38.4%; H, 4.17%; N, 7.90%. Found: C, 38.1%; H, 4.32%; N, 8.06%. $PefH_2[ZnBr_4]$ (**3**) and $PefH_2[ZnCl_4]$ (**4**) was prepared according to the previously described methods [26,27]. The elemental analysis for $C_{17}H_{22}Br_4FN_3O_3Zn$ (**3**): Calc.: C, 28.3%; H, 3.08%; N, 5.83%. Found: C, 28.1%; H, 2.82%; N, 5.66%. The elemental analysis for $C_{17}H_{22}Cl_4FN_3O_3Zn$ (**4**): Calc.: C, 37.6%; H, 4.09%; N, 7.74%. Found: C, 37.2%; H, 3.88%; N, 7.56%.

2.3. X-ray diffraction analysis

The intensity patterns were collected from single crystals $PefH_2[MnBr_4]$ (**1**) and $PefH_2[MnCl_4]$ (**2**) at 296 K using a Bruker AXS SMART APEX II single crystal diffractometer equipped with a CCD-detector, graphite monochromator and Mo Kα radiation source. The absorption corrections were applied using the SADABS program. The structures were solved by the direct methods using package SHELXT and refined in the anisotropic approach for all non-hydrogen atoms using the SHELXL program [28]. All hydrogen atoms of the $PefH_2^{2+}$ ions were positioned geometrically as riding on their parent atoms with d(C–H) = 0.97 Å for the C–H bonds and d(N–H)=0.89 Å for all other N–H bonds and $U_{iso}(H) = 1.2U_{eq}(C,N)$. The structure test for the presence of missing symmetry elements and possible voids was produced using the PLATON program [29]. The parameters of crystal structure for **1** and **2** are shown in Table 1. The coordinates of atoms are in Table S1, Table S2, main bond lengths are given in Table S3. The DIAMOND program [30] is used for the crystal structure plotting (Fig. 1). Powder X-ray diffraction data of **1**-**4** were collected at room temperature with a Bruker D8 ADVANCE powder diffractometer using Cu Kα radiation and linear VANTEC detector with a Ni filter. All peaks were indexed by monoclinic cell ($P2_1/c$) with parameters close to ones obtained from single crystal. These parameters were taken as starting model for Le Bail profile fitting which was performed using TOPAS 4.2 [31]. Refinements gave low *R*-factors proving that bulk materials were pure (Fig. S1, Table S4).

2.4. Measurements of physico-chemical properties

Thermogravimetric (TG) and differential scanning calorimetry (DSC) analysis of synthesized compounds **1** and **2** was carried out on a NETZSCH STA 409 PC/PG Thermal Analyzer under the dynamic argon atmosphere (15 ml/min flow rate) within 25–600°C at the scan rate of 10°C/min. The sample weight was 26.620 mg for **1** and 9.830 mg for **2**. Platinum crucibles with perforated lids were used as containers. The chemical analysis was performed with a HCNS-0 EA 1112 Flash Elemental Analyzer.

2.5. Measurements of photoluminescent properties

The photoluminescence (PL) and photoluminescence excitation (PLE) spectra of powders **1**-**4** as well as the PL decays on the microsecond time scale were recorded on a Horiba Scientific Fluorolog 3–22 spectrofluorometer. The emission for decays was collected at the wavelength of 445 and 520 nm from flash lamp; the delay time was 60 μs. The measurements of PL spectra of powders were carried out at different excitation wavelengths of 320-500 nm. The PL spectra were corrected to the following distorting factors: spectral sensitivity of PMT, different intensity of excitation, and the background. All spectral measurements were performed at a room temperature using the front face geometry. Under experimental conditions, the samples were stable to the UV irradiation.

Table 1
The parameters of crystal structure for **1** and **2**.

Chemical formula	$C_{17}H_{22}Br_4FMnN_3O_3$	$C_{17}H_{22}Cl_4FMnN_3O_3$
Molecular weight	709.95	532.11
Temperature (K)	296(2)	296(2)
Space group, *Z*	$P2_1/c$	$P2_1/c$
a (Å)	14.3099(5)	14.0713(4)
b (Å)	12.4183(4)	12.0626(3)
c (Å)	13.6155(4)	13.2988(4)
β (°)	90.2681(8)	90.8350(10)
V (Å^3)	2419.51(14)	2257.05(11)
ρ_{calc} (g/cm^3)	1.949	1.566
μ (mm^{-1})	7.181	1.090
Reflections measured	37164	33340
Reflections independent	7895	7005
Reflections with $F > 4\sigma(F)$	5260	4873
$2\theta_{max}$ (°)	62.70	61.40
h, k, l - limits	$-20 \le h \le 20$; $-18 \le k \le 18$; $-19 \le l \le 19$	$-20 \le h \le 20$; $-17 \le k \le 17$; $-19 \le l \le 19$
R_{int}	0.0455	0.0517
Refinement results		
The weighed refinement of F^2	$w=1/[\sigma^2(F_o^2)+(0.0274P)^2+1.0312P]$ where $P=\max(F_o^2+2F_c^2)/3$	$w=1/[\sigma^2(F_o^2)+(0.0582P)^2+0.9352P]$ where $P=\max(F_o^2+2F_c^2)/3$
Number of refinement parameters	268	268
*R*1 [$F_o > 4\sigma(F_o)$]	0.0344	0.0389
wR2	0.0660	0.0967
Goof	1.026	0.918
$\Delta\rho_{max}$ (e/Å^3)	1.039	0.303
$\Delta\rho_{min}$ (e/Å^3)	-0.630	-0.281
$(\Delta/\sigma)_{max}$	0.077	0.056
Extinction coefficient (SHELXL 2014/7)	none	none

The photoluminescence quantum yield (PLQY) of polycrystals **1-4** was measured using a Newport integrating sphere RTC-060-SF, an Ocean Optics spectrometer Maya2000 with fiber-optic input and three LEDs: L365A, L405A (Ocean Optics) and one standard LED peaking 450 nm. The reliability of PLQY values measured with Maya200 spectrometer and Newport integrating sphere were approved using Qauntarus-QY absolute quantum yield spectrometer. The differences were within three standard errors for all samples, which means that good reliability of experimental data was obtained. The standard YAG:Ce^{3+} powder sample from factory, which was measured recently, showed 98 ± 1 % under 450 nm excitation (real values should be 98-100 %).

3. Results and discussion

3.1. Crystal structures of *1* and *2*

The asymmetric part of the $PefH_2[MnBr_4]$ and $PefH_2[MnCl_4]$ unit cell contains one of $PefH_2^{2+}$ ($C_{17}H_{22}FN_3O_3^{2+}$), one Mn^{2+} and four Br^-/Cl^- ions. The Mn^{2+} ion is coordinated by four Br^-/Cl^- ions forming $Mn(Br/Cl)_4$ distorted tetrahedron (Fig. 1) with bond lengths between 2.4726(5) and 2.5337(5) Å for **1**, 2.3272 (7) and 2.3927 (7) Å for **2** (Table S3). The Mn—Br bond lengths in **1** slightly longer then the Mn—Cl bond lengths in **2** due to the larger radius of the bromide ion. The X—Mn—X angles are varied from 106.130(19) to 113.597(18)° for **1** and 105.43(2) to 115.48(3)° for **2**. These values are close to those found in the reported $Mn(Br/Cl)_4$ tetrahedrons [11–21]. These tetrahedrons are isolated from each other by bulky $PefH_2^{2+}$ ions. The closest Mn···Mn distance within the crystal is 7.3300(5) Å for **1** and 7.2727(5) Å for **2**. Due to the similarity of compounds **1** and **2**, only the structure of **1** was described. Double protonated $PefH_2^{2+}$ (pefloxacindi-ium) ion is formed only in extremely acidic conditions [32], which corresponds to the conditions of the synthesis. The $PefH_2^{2+}$ contains a protonated carboxyl group, a protonated N3 atom of the piperazinyl ring, and a protonated carbonyl atom O1 (Figs. 1,2). All values of bond lengths and bond angles in $PefH_2^{2+}$ ions are in good agreement with those obtained in other compounds [26,33–37]. Two intramolecular O1—HO1···O2 and C14—H14A···F hydrogen bonds are presented in the structure (Fig. 1). The intermolecular N3—H3···Br1 and O3—H···Br2 hydrogen bonds form zigzag chains, each of which consists of the alternating $PefH_2^{2+}$ and Br^- ions. These interactions together with weaker C—H···O and C—H···Br hydrogen bonds (Figs. 1, 2, Tables S5, S6) form a three-dimensional network. All bromide ions are involved in hydrogen bonding. Two $PefH_2^{2+}$ ions from neighboring chains are linked by $\pi-\pi$ interaction of the "head-to-tail" type (Fig. 2, Table S7), and neighboring $PefH_2^{2+}$ ions located in the same chain are linked by $\pi-\pi$ interaction with $PefH_2^{2+}$ ions from the different chains.

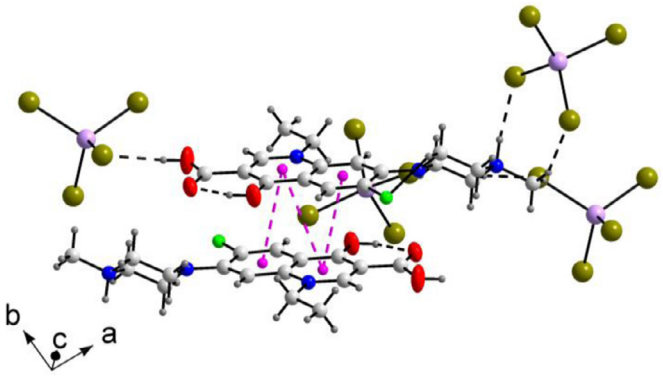

Fig. 2. Hydrogen bonds and $\pi-\pi$ interactions in $PefH_2[MnBr_4]$ (**1**).

3.2. Thermal decomposition of *1* and *2*

To know general stability, the thermal decomposition was implemented for synthesized compounds. The TG and DSC curves measured in argon (Figs. S2, S3) indicate the thermal stability of samples **1** and **2** up to 230°C and 210°C respectively. The TG and DSC curves are similar for Mn(II) compounds and show at least three-step decomposition accompanied by several endo and exo effects. The strong endo effect is observed at 279°C for **1** and

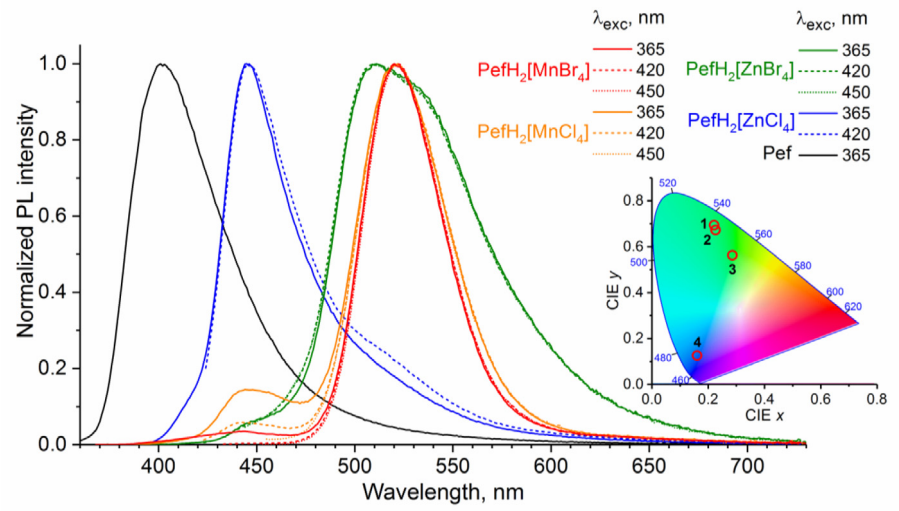

Fig. 3. PL spectra of powders **1**-**4** under different excitation. Insertion: The position of powders **1**-**4** in CIE coordinates are indicated.

Table 2
PL properties of powders under excitation of 365 nm at room temperature.

Powder	λ_{exc_max}, nm[a]	λ_{PL_max}, nm[b]	FWHM, nm[c]
$PefH_2[MnBr_4]$ (**1**)	453; 427; 362; 340	521	48
$PefH_2[MnCl_4]$ (**2**)	410; 363; 341	521	52
$PefH_2[ZnBr_4]$ (**3**)	418; 363, 340	510	84
$PefH_2[ZnCl_4]$ (**4**)	420; 362; 340	445	44
Pef	360; 340	402	56

[a] λ_{exc_max} is the wavelength of peaks and obvious shoulders in PLE spectrum.
[b] λ_{PL_max} is the wavelength of maximum of PL spectrum.
[c] FWHM is full width at half maximum of PL spectrum.

276 °C for **2**. The first stage of decomposition of **1** proceeded in the range of 230-310°C and showed the weight loss (Δm) equal to ~12.6% (Fig. S2), which is best consistent with the loss of one HBr molecule by the compound (Δm_{theor} = 11.4%). The thermal decomposition of **2** presumably starts with the removal of two easily volatile HCl molecules.

3.3. Photoluminescent properties

3.3.1. PL and PLE spectra

The powders **1**-**3** exhibit green luminescence under excitation, while powder **4** has blue luminescence (see photographs in SI, Fig. S4). The PL spectra of powders **1**-**4** under different excitation in the range of 365–450 nm are shown in Fig. 3 with insertion of chromaticity coordinates. The calculated CIE coordinates of PL spectra are given separately for polycrystals **1**-**4** in Fig. S5 and equal to (0.22, 0.69), (0.22, 0.67), (0.28, 0.56) and (0.16, 0.12) respectively.

The luminescent parameters of powders **1**-**4** are presented in Table 2. The PL spectra of Mn(II) compounds **1**-**2** consists of pronounced green band with a maximum at 521 nm and weak blue band at 445 nm. The green band of emission is independent of the nature of halide ion, in contrast to the blue band, which is more intense in the case of chloride than bromide. In this case, the chloride compound gives a wider green band (FWHM = 52 nm) as compared to the bromide one (FWHM = 48 nm). The intensity redistribution of blue and green bands at 445 and 521 nm depends on the excitation wavelength. At λ_{exc} > 450 nm, the blue band in emission of **1**-**2** disappears.

For Zn(II) compounds **3** and **4**, the effect of halide ion is more significant: chloride (**4**) gives blue PL with a rather narrow band (FWHM = 44 nm) centered at 445 nm and weak shoulder in the long-wavelength region of the spectrum (500–600 nm), while bromide (**3**) gives a broader band (FWHM = 84 nm) with the peak at 510 nm corresponding to the strong green PL and small shoulder around 445 nm. Moreover, the shape of the PL spectrum for Zn(II) compounds does not depend on the excitation wavelength, that is, the contribution of the blue and green bands remains constant, in contrast to Mn(II) compounds **1** and **2**, where the shoulder at 445 nm disappears at λ_{exc} > 450 nm.

In emission blue and green bands measured at 445 and 520 nm the photoluminescence excitation spectra were obtained and presented in Fig. 4; PLE parameters are given in Table 2. The PLE spectrum of Pef has the broad bands with peaks around 340 and 360 nm. Similar broad bands of Pef are observed in the PLE spectra of all compounds containing metals **1**-**4**. The band at about 420 nm reveals the different intensities for compounds **1**-**4**, while Pef does not have this band. PLE spectra of **1** and **2** is characterized by the appearance of additional intensive broad band and weak shoulder near 450 nm respectively (Fig. 4). PLE spectra of **3** and **4** contain only a band at about 420 nm of varying intensity.

The PLE spectra of Mn(II) complexes **1-2** could consist of the different overlapping bands from the MnX_4^{2-} and $PefH_2^{2+}$ ions, therefore their correct assignment is difficult [38]. From Ref. [16], the PLE spectra in the blue and near-ultraviolet region of Mn(II) complexes exhibit several bands, formally corresponding to two groups of transitions: $^6A_1 \rightarrow {}^4G$ and $^6A_1 \rightarrow {}^4D$.

3.3.2. Origin of photoluminescence and PLQY

For powders **1**-**4**, the photoluminescence band at around 445 nm could be attributed to the Pef emission, which has the maximum at 402 nm (Fig. 3) in the solid state, and the green band – to manganese or MLCT/LMCT excited states of metals [6,14,39–42]. Unlike powder, the emission spectrum of Pef in aqueous solution is pH dependent and changes upon different excitation wavelengths. At 300 nm excitation, PL spectra of pefloxacin in aqueous solution exhibit two emission bands with maxima around 450 and 500 nm [24], which can also be traced for the PL spectra of solid compounds **1**-**4**. With acidity increase, the long-wavelength maximum at 500 nm is redshifted [24]. Hence, we could attribute the green luminescence of **1** and **2** at 521 nm mainly to single exciton emission of $PefH_2^{2+}$ cations, since the optical properties of self-assembled metal halides are similar to pure pefloxacin in aqueous solution. This assumption is supported by the PL of hybrid metal halides with another fluoroquinolone [30], enrofloxacin, which has a similar composition and structure to pe-

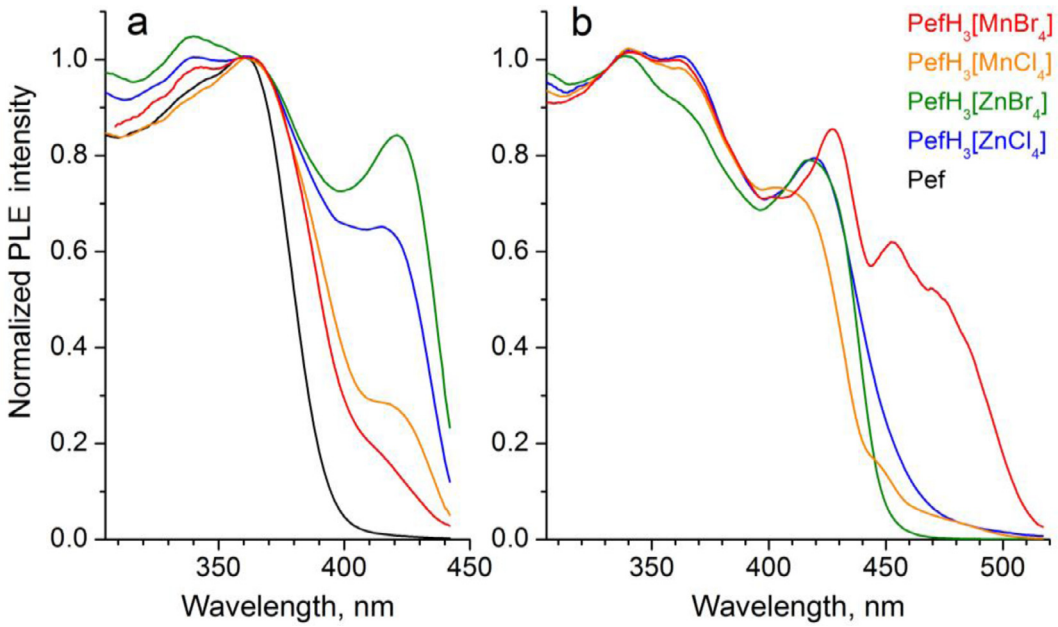

Fig. 4. PLE spectra of powders **1**-**4** measured at (a) blue (445 nm) and (b) green (520 nm) bands of PL spectra. For comparison, the PLE spectrum for Pef powder is shown.

floxacin (Fig. S6). The density functional theory calculations indicated that the emission of enrofloxacindi-ium *p*-metal (Pb^{2+}, Bi^{3+} and Sn^{4+}) chlorides originates from organic cations [43]. The photoluminescence maximum of these compounds is at 443–465 nm. The intensity of PL spectra is affected by the nature of the metal. Among the isostructural compounds **1**-**4**, only $PefH_2[ZnCl_4]$ (**4**) exhibits the same blue luminescence at 445 nm. The weak shoulder of this band is also observed in the short-wavelength region of the PL spectrum for **1**-**3** (Fig. 3).

As shown in Fig. 3, PL spectrum of $PefH_2[ZnBr_4]$ isostructural to $PefH_2[MnBr_4]$ reveals two green bands at 510 nm and near 540 nm, although it does not contain the manganese(II) ion. In zinc compounds with π-conjugated organic $PefH_2^{2+}$ cations, the energy of the metal orbitals is very high [40–42], and the excitation is most likely concentrated on $PefH_2^{2+}$. Alternatively, for Zn(II) complexes the luminescence could originate from the excited states of MLCT/LMCT, for example, for some of them the phosphorescence has been reported due to LMCT mechanism involving the low-lying empty s- and p-orbitals [6,7,44–46]. The observed difference in PL spectra of **3** and **4** is a consequence of the strong influence of the halide ion on the optical properties of $PefH_2^{2+}$ and/or LMCT excited states of Zn(II). On the contrary, the nature of the halide ion does not affect the position of photoluminescence maximum of compounds **1** and **2** (Fig. 3, Fig. S5), which is also consistent with a little effect of the Cl^- ion by Br^- replacement in hybrid manganese(II) tetrahalides [16]. The luminescent properties of isostructural compounds **1** and **2** are very similar to the described tetrachloromanganese(II) compounds [12,16,18], which all follow the well-known rule: for tetrahedrally coordinated Mn(II) compounds, the emission is observed at around 520 nm. This assumes that the Mn^{2+} ions can emit green light due to the $^4T_1(G) \rightarrow {}^6A_1$ transition [12] which is added to the green luminescence of organic $PefH_2^{2+}$ ions.

In our synthesized compounds, we rule out the possibility of self-trapped exciton (STE) formation which was generally observed in low dimensional hybrid metal halides. In the case of STEs formation, FWHM is very broad (> 100 nm) for a single emission peak [15]. The FWHM values for **1**-**4** are 44-84 nm (Table 2). The difference between two hybrid manganese(II) halides lies in the intensity of green emission.

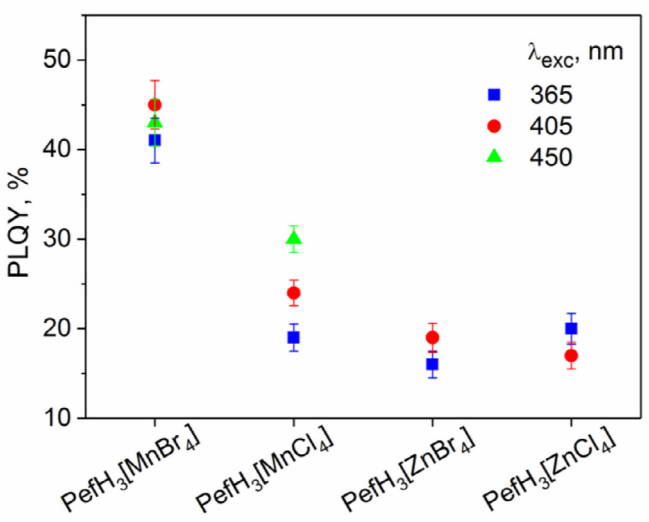

Fig. 5. The PLQY measured at different excitation wavelengths.

For powders **1, 3** and **4** measured PLQY is not dependent on excitation wavelength (Fig. 5) and equal to 43 ± 2%, 16 ± 2%, 19 ± 2% respectively. For **2** PLQY increase from 19 to 30% with excitation wavelength from 365 to 450 nm. It could be suggested that this difference in PLQY is associated with the redistribution of the blue and green bands in the PL spectrum (Fig. 3). At 365 nm excitation, both $PefH_2^{2+}$ cations and Mn^{2+} ions emit, therefore the average PLQY is low due to the contribution of weak fluorescent $PefH_2^{2+}$ cations. At 450 nm excitation, only Mn^{2+} ions are excited, which explains the higher PLQY of compounds **1** and **2**. The PLQY of Mn(II) compounds decreases from bromide (**1**) to chloride (**2**).

3.3.3. Photoluminescence lifetimes

The nanosecond time-resolved PL decays of Pef and powders **1, 3** were measured with the help of Horiba Scientific module FluoroHub A and spectrofluorometer Fluorolog 3-22 at excitation of 373 nm from NanoLED. The lifetimes obtained by deconvolution in

the DAS software are given in Table S8. The lifetime of Pef powder is 0.83 ns, which corresponds to the range of fluorescence lifetimes. For other fluoroquinolone, enrofloxacin, the powder lifetime is 2.77 ns [43]. For compounds with metals **1** and **3**, the lifetimes dramatically decrease to 0.02-0.05 ns. This could indicate that the introduction of metal enhances the nonradiative relaxation of the fluorescent excited state of Pef either to the triplet state or to the excited states of manganese and zinc metal ions.

The time-resolved PL spectra of Pef and compounds **1**-**4** measured under microsecond excitation reveal the maximum at around 510-540 nm for all powders (Fig. S7). The PL lifetimes obtained by the single or double exponential fit of decays are shown in Table S9. The lifetimes of about 4.2–4.9 ms detected at 520 nm for Pef and Zn(II) compounds **3, 4** are similar. The significantly shorter lifetimes of 0.47 and 1.23 ms are determined for Mn(II) compounds **1** and **2**, which is consistent with the Mn^{2+} emission. Thus, the PL lifetime of 0.35 ms is reported in [15] for the similar type of hybrid manganese(II) bromides. It should be noted that both the fluorescence and phosphorescence are observed for Pef and metal compounds **1-4** (Table S8, S9). The fluorescence and phosphorescence arise from $PefH_2^{2+}$ centered molecular orbitals, while phosphorescence can also involves the LMCT mechanism as well as the $^4T_1(G) \rightarrow {}^6A_1$ transition for Mn(II) compounds.

For **1** and **2**, the effect of halide ion on lifetime is observed: 2.6-fold decrease from Cl^- to Br^-. This could be the result of the enhancement of spin-orbit interaction upon the introduction of heavy atoms into the crystal structure. The spin-orbit coupling constant for halogens is 2460 cm^{-1} for Br, 587 cm^{-1} for Cl [47] and for metal ions is 300 cm^{-1} for Mn^{2+}, ~1000 cm^{-1} for Zn^{2+} [48]. The influence of halide ion on the PL lifetime and thus on emission centers suggests that in **1** and **2**, along with $PefH_2^{2+}$ ions, Mn^{2+} ions emit. For Zn(II) compounds **3** and **4**, the lifetime is independent of halide ion, which is consistent with the predominant emission of $PefH_2^{2+}$ ions. However, as noted above, the contribution of other luminescence pathways, for example, including an LMCT mechanism cannot be excluded, especially considering the broadness of the PL spectrum of $PefH_2[ZnBr_4]$ (**3**). Thus, the differences in the parameters of the PL spectra and decays as well as the effect of halide ion on the luminescence for the isostructural Mn(II) and Zn(II) compounds, are in good agreement with the assumption that the PL in **1** and **2** originates from manganese(II).

4. Conclusions

Two lead-free zero-dimensional organic-inorganic hybrid compounds $PefH_2[MnBr_4]$ (**1**) and $PefH_2[MnCl_4]$ (**2**) with moderate PLQY and high thermal stability are synthesized and structurally characterized. In crystal structure, the $[MnX_4]^{2-}$ anions interact with the organic $PefH_2^{2+}$ cations through the network of hydrogen bonding. The structures are additionally stabilized by head-to-tail π–π stacking interactions between pefloxacindi-ium ions. The photoluminescence of **1**-**2** is attributed to the single exciton emission of $PefH_2^{2+}$ cations and to the emission from the $^4T_1(G) \rightarrow {}^6A_1$ transition of Mn^{2+} ions. We also found that the maximum of green luminescence band of Mn(II) compounds is independent of the halide ion nature and the excitation wavelength, but only for **2** PLQY varies with the excitation wavelength. It is assumed that the compounds **3** and **4** contain excited states of $PefH_2^{2+}$-centred and/or $PefH_2^{2+}$-to-Zn(II) charge transfer nature, the coexistence of which can produce both short-lived and long-lived emissions. For Zn(II) compounds, the maximum of PL spectra strongly depends on the halide ion nature. Thus, the substitution methodology of halide and metal ion in isostructural HMHs provides a strong synthetic handle to further tune the emission profile (and CIE coordinates) retaining moderate PLQY.

Supplementary information

The crystallographic data (excluding structure factors) for the structural analysis have been deposited with Cambridge Crystallographic Data Centre (**1** - CCDC # 2081472; **2** - CCDC # 2081473). The information may be obtained free of charge from The Director, CCDC, 12 Union Road, Cambridge CB2 1EZ, UK (Fax: +44(1223)336-033, E-mail: deposit@ccdc.cam.ac.uk, or www: www.ccdc.cam.ac.uk).

Declaration of Competing Interest

The authors declare that they have no known competing financial interests or personal relationships that could have appeared to influence the work reported in this paper.

CRediT authorship contribution statement

Nicolay N. Golovnev: Conceptualization, Supervision, Writing – review & editing. **Marina A. Gerasimova:** Investigation, Data curation, Formal analysis, Supervision, Writing – review & editing. **Maxim S. Molokeev:** Investigation, Data curation, Formal analysis, Supervision, Project administration, Writing – review & editing. **Mikhail E. Plyaskin:** Investigation, Data curation, Formal analysis. **Mikhail E. Baronin:** Investigation, Data curation, Formal analysis.

Acknowledgements

This work is supported by the RFBR according to the research project № 19-52-80003. The use of equipment of Krasnoyarsk Regional Center of Research Equipment of Federal Research Center "Krasnoyarsk Science Center SB RAS" is acknowledged.

Supplementary materials

Supplementary material associated with this article can be found, in the online version, at doi:10.1016/j.molstruc.2021.131468.

References

[1] M.M. Lee, J. Teuscher, T. Miyasaka, T.N. Murakami, H.J. Snaith, Efficient hybrid solar cells based on meso-superstructured organometal halide perovskites, Science 338 (2012) 643–647, doi:10.1126/science.1228604.
[2] B. Saparov, D.B. Mitzi, Organic-inorganic perovskites: structural versatility for functional materials design, Chem. Rev. 116 (2016) 4558–4596, doi:10.1021/acs.chemrev.5b00715.
[3] O.F. Mohammed, Outstanding challenges of zero-dimensional perovskite materials, J. Phys. Chem. Lett. 10 (2019) 5886–5888, doi:10.1021/acs.jpclett.9b00175.
[4] M.D. Smith, B.A. Connor, H.I. Karunadasa, Tuning the luminescence of layered halide perovskites, Chem. Rev. 119 (2019) 3104–3139, doi:10.1021/acs.chemrev.8b00477.
[5] P. Billen, E. Leccisi, S. Dastidar, S. Li, L. Lobaton, S. Spatari, A.T. Fafarman, V.M. Fthenakis, J.B. Baxter, Comparative evaluation of lead emissions and toxicity potential in the life cycle of lead halide perovskite photovoltaics, Energy 166 (2019) 1089–1096, doi:10.1016/j.energy.2018.10.141.
[6] C. Bizzarri, E. Spuling, D.M. Knoll, D. Volz, S. Bräse, Sustainable metal complexes for organic light-emitting diodes (OLEDs), Coord. Chem. Rev. 373 (2018) 49–82, doi:10.1016/j.ccr.2017.09.011.
[7] O.S. Wenger, Photoactive complexes with earth-abundant metals, J. Am. Chem. Soc. 140 (2018) 13522–13533, doi:10.1021/jacs.8b08822.
[8] P. Singh, P.J.S. Rana, P. Dhingra, P. Kar, Towards toxicity removal in lead based perovskite solar cells by compositional gradient using manganese chloride, J. Mater. Chem. C 4 (2016) 3101–3105, doi:10.1039/C6TC00650G.
[9] L.-J. Xu, C.-Z. Sun, H. Xiao, Y. Wu, Z.-N. Chen, Green-light-emitting diodes based on tetrabromide manganese(II) complex through solution process, Adv. Mater. 29 (2017) 1605739, doi:10.1002/adma.201605739.
[10] F.A. Cotton, D.M.L. Goodgame, M. Goodgame, Absorption spectra and electronic structures of some tetrahedral manganese(II) complexes, J. Am. Chem. Soc. 84 (1962) 167–172, doi:10.1021/ja00861a008.
[11] S. Chen, J. Gao, J. Chang, Zhang Y, L. Feng, Organic-inorganic manganese (II) halide hybrids based paper sensor for the fluorometric determination of pesticide ferbam, Sensor. Actuat. B-Chem. 297 (2019) 126701, doi:10.1016/j.snb.2019.126701.

[12] H. Yu, Y.X. Mei, Z.H. Wei, G.Q. Mei, H. Cai, Fluorescent properties of manganese halide benzothiazole inorganic-organic hybrids, J. Fluoresc. 26 (2016) 2295–2301, doi:10.1007/s10895-016-1925-x.
[13] S. Wang, X. Han, T. Kou, Y. Zhou, Y. Liang, Z. Wu, J. Huang, T. Chang, C. Peng, Q. Wei, B. Zou, Lead-free Mn^{II}-based red-emitting hybrid halide $(CH_6N_3)_2MnCl_4$ toward high performance warm WLEDs, J. Mater. Chem. C 9 (2021) 4895–4902, doi:10.1039/D1TC00632K.
[14] Y-L. Wei, J. Jing, C. Shi, H.-Y. Ye, Z.-X. Wang, Y. Zhang, High quantum yield and unusual photoluminescence behaviour in tetrahedral manganese(II) based on hybrid compounds, Inorg. Chem. Front. 5 (2018) 2615–2619, doi:10.1039/C8QI00793D.
[15] A. Jana, S. Zhumagali, Q. Ba, A.S. Nissimagoudar, K.S. Kim, Direct emission from quartet excited states triggered by upconversion phenomena in solid-phase synthesized fluorescent lead-free organic-inorganic hybrid compounds, J. Mater. Chem. A 7 (2019) 26504–26512, doi:10.1039/C9TA08268A.
[16] V. Morad, I. Cherniukh, L. Pöttschacher, Y. Shynkarenko, S. Yakunin, M.V. Kovalenko, Manganese(II) in tetrahedral halide environment: factors governing bright green luminescence, Chem. Mater. 31 (2019) 10161–10169, doi:10.1021/acs.chemmater.9b03782.
[17] B. Su, G. Zhou, J. Huang, E. Song, A. Nag, Z. Xia, Mn^{2+}-Doped metal halide perovskites: structure, photoluminescence, and application, Laser Photonics Rev. 15 (2021) 2000334, doi:10.1002/lpor.202000334.
[18] C. Jiang, H. Fu, Y. Han, D. Li, H. Lin, B. Li, X. Meng, H. Peng, J. Chu, Tuning the crystal structure and luminescence of pyrrolidinium manganese halides via halide ions, Cryst. Res. Tech. 54 (2019) 1800236, doi:10.1002/crat.201800236.
[19] Y. Rodríguez-Lazcano, L. Nataf, F. Rodríguez, Electronic structure and luminescence of $[(CH_3)_4N]_2MnX_4$ (X=Cl,Br) crystals at high pressures by time-resolved spectroscopy: pressure effects on the Mn-Mn exchange coupling, Phys. Rev. B Condens. Matter 80 (2009) 085115, doi:10.1103/PhysRevB.80.085115.
[20] S. Pitula, A.-V. Mudring, Synthesis, structure, and physico-optical properties of manganate(II)-based ionic liquids, Chem. Eur. J. 16 (2010) 3355–3365.
[21] K. Nikolič, F. Lignou, H.P. de la Garanderie, Luminescence spectra in tetrahalomanganate complexes, J. Lumin. 8 (1973) 137–148, doi:10.1016/0022-2313(73)90100-2.
[22] C. Jiang, N. Zhong, C. Luo, H. Lin, Y. Zhang, H. Peng, C.-G. Duan, Diisopropylammonium)$_2MnBr_4$: a multifunctional ferroelectric with efficient green-emission and excellent gas sensing properties, Chem. Commun. 53 (2017) 5954–5957, doi:10.1039/C7CC01107E.
[23] A.S. Berezin, M.P. Davydova, D.G. Samsonenko, T.S. Sukhikh, A.V. Artem'ev, A family of brightly emissive homo- and mixed-halomanganates(II): the effect of halide on optical and magnetic properties, J. Lumin. 236 (2021) 118069, doi:10.1016/j.jlumin.2021.118069.
[24] A.I. Drakopoulos, P.C. Ioannou, Spectrofluorimetric study of the acid-base equilibria and complexation behavior of the fluoroquinolone antibiotics ofloxacin, norfloxacin, ciprofloxacin and pefloxacin in aqueous solution, Anal. Chim. Acta 354 (1997) 197–204, doi:10.1016/S0003-2670(97)00465-0.
[25] K. Žamojć, W. Wiczk, B. Zaborowski, M. Makowski, J. Pranczk, D. Jacewicz, L. Chmurzyński, Fluorescence quenching of fluoroquinolone antibiotics by 4-hydroxy-TEMPO in aqueous solution, Spectrochim. Acta A 133 (2014) 887–891, doi:10.1016/j.saa.2014.06.127.
[26] A.D. Vasil'ev, N.N. Golovnev, Crystal structure of pefloxancindium tetrabromidozinkate $C_{17}H_{22}FN_3O_3^{2+} \cdot ZnBr_4^{2-}$, Russ. J. Inorg. Chem. 57 (2012) 248–251, doi:10.1134/S0036023612020271.
[27] N.N. Golovnev, N.G. Naumov, A.A. Bakhtina, A.O. Lykhin, Crystal structure of a new compound $C_{17}H_{22}FN_3O_3^{2+} \cdot ZnCl_4^{2-}$, J. Struct. Chem. 51 (2010) 980–983, doi:10.1007/s10947-010-0151-7.
[28] G.M. Sheldrick, Crystal structure refinement with SHELXL, Acta Cryst. C 71 (1) (2015) 3–8, doi:10.1107/S2053229614024218.
[29] PLATONA Multipurpose Crystallographic Tool, Utrecht University, Utrecht, The Netherlands, 2008.
[30] K. Brandenburg, M. Berndt, DIAMOND – visual crystal structure information system CRYSTAL IMPACT, Postfach 1251, D-53002 Bonn.
[31] Bruker AXS TOPAS V4: General profile and structure analysis software for powder diffraction data. – user's manual, Bruker AXS, Karlsruhe, Germany (2008).
[32] I. Turel, The interactions of metal ions with quinolone antibacterial agents, Coord. Chem. Rev. 232 (2002) 27–47, doi:10.1016/S0010-8545(02)00027-9.
[33] N.N. Golovnev, M.S. Molokeev, M.K. Lesnikov, I.V. Sterkhova, V.V. Atuchin, Thiobarbiturate and barbiturate salts of pefloxacin drug: growth, structure, thermal stability and IR-spectra, J. Mol. Struct. 1149 (2017) 367–372, doi:10.1016/j.molstruc.2017.08.011.
[34] N.N. Golovnev, N.G. Naumov, I.I. Golovneva, N.V. Dorokhova, Structure of $(C_{17}H_{22}FN_3O_3)[MCl_4]\cdot H_2O$ (M = Cd, Hg), J. Struct. Chem. 52 (2011) 1003–1007, doi:10.1134/S0022476611050271.
[35] A.D. Vasiliev, N.N. Golovnev, Synthesis and structure of $C_{17}H_{22}FN_3O_3^{2+}\cdot CuCl_4^{2-}$, J. Struct. Chem. 51 (2010) 177–180, doi:10.1007/s10947-010-0026-y.
[36] A.D. Vasiliev, N.N. Golovnev, Structure of the oxonium compound of pefloxacinium hexachloridostannate (IV), J. Struct. Chem. 59 (2018) 641–645, doi:10.1134/S0022476618030198.
[37] L.A. Mitsher, Bacterial topoisomerase inhibitors: quinolone and pyridone antibacterial agents, Chem. Rev. 105 (2005) 559–592, doi:10.1021/cr030101q.
[38] I. Buric, K. Nikolic, A. Aleksic, Excitation-spectra of tetrahedral complex-compounds of manganese(ii) bromide with hydrobromides of some derivatives of pyridine and pyperidine, Czech. J. Phys. 27 (1977) 224–232.
[39] Y. Qin, P. She, X. Huang, W. Huang, Q. Zhao, Luminescent manganese(II) complexes: Synthesis, properties and optoelectronic applications, Coord. Chem. Rev. 416 (2020) 213331, doi:10.1016/j.ccr.2020.213331.
[40] M.B. Bushuev, B.A. Selivanov, N.V. Pervukhina, D.Y. Naumov, L.A. Sheludyakova, M.I. Rakhmanova, A.Y. Tikhonov, S.V. Larionov, Zinc(II) complexes with an imidazolylpyridine ligand: Luminescence and hydrogen bonding, J. Coord. Chem. 67 (2014) 611–622, doi:10.1080/00958972.2014.892589.
[41] A. Yangui, R. Roccanova, T.M. McWhorter, Y. Wu, M.-H. Du, B. Saparov, Hybrid organic–inorganic halides $(C_5H_7N_2)_2MBr_4$ (M = Hg, Zn) with high color rendering index and high-efficiency white-light emission, Chem. Mater. 31 (2019) 2983–2991, doi:10.1021/acs.chemmater.9b00537.
[42] M.M. Radanović, M.G. Jelić, N.Ž. Romčević, N. Boukos, L.S. Vojinović-Ješić, V.M. Leovac, B.B. Hadžić, B.M. Bajac, L.F. Nađ, C. Chandrinou, Synthesis, structure and photoluminescence of $(PLAGH)_2[ZnCl_4]$ and comparative analysis of photoluminescence properties with tris(2,2′-bipyridine)ruthenium(II), Mater. Res. Bull. 70 (2015) 951–957, doi:10.1016/j.materresbull.2015.06.034.
[43] B. Su, G. Song, M.S. Molokeev, N.N. Golovnev, M.K. Lesnikov, Z. Lin, Z. Xia, Role of metal-chloride anions in photoluminescence regulations for hybrid metal halides, J. Phys. Chem. Lett. 12 (2021) 1918–1925, doi:10.1021/acs.jpclett.1c00182.
[44] A. Barbieri, G. Accorsi, N. Armaroli, Luminescent complexes beyond the platinum group: the d^{10} avenue, Chem. Commun. (2008) 2185–2193, doi:10.1039/b716650h.
[45] Q.-D. Liu, R. Wang, S. Wang, Blue phosphorescent Zn(II) and orange phosphorescent Pt(II) complexes of 4,4′-diphenyl-6,6′-dimethyl-2,2′-bipyrimidine, Dalton Trans 14 (2004) 2073–2079, doi:10.1039/B404905E.
[46] J. Cepeda, E.S. Sebastian, D. Padro, A. Rodrıguez-Dieguez, J.A. Garcı, J.M. Ugalde, J. Seco, A Zn based coordination polymer exhibiting long-lasting phosphorescence, Chem. Commun. 52 (2016) 8671–8674, doi:10.1039/C6CC03242G.
[47] D.S. McClure, Triplet-singlet transitions in organic molecules. Lifetime measurements of the triplet state, J. Chem. Phys. 17 (1949) 905–913, doi:10.1063/1.1747085.
[48] T.M. Dunn, Spin-orbit coupling in the first and second transition series, Trans. Faraday Soc. 57 (1961) 1441–1444, doi:10.1039/TF9615701441.